Multi-Scale Adaptive Network for Single Image Denoising

Yuanbiao Gou[1], **Peng Hu**[1], **Jiancheng Lv**[1], **Joey Tianyi Zhou**[2], **Xi Peng**[1*]
[1]College of Computer Science, Sichuan University, China.
[2]Institute of High Performance Computing, A*STAR, Singapore.
{gouyuanbiao, penghu.ml, joey.tianyi.zhou, pengx.gm}@gmail.com
lvjiancheng@scu.edu.cn

Abstract

Multi-scale architectures have shown effectiveness in a variety of tasks thanks to appealing cross-scale complementarity. However, existing architectures treat different scale features equally without considering the scale-specific characteristics, *i.e.*, the within-scale characteristics are ignored in the architecture design. In this paper, we reveal this missing piece for multi-scale architecture design and accordingly propose a novel Multi-Scale Adaptive Network (MSANet) for single image denoising. Specifically, MSANet simultaneously embraces the within-scale characteristics and the cross-scale complementarity thanks to three novel neural blocks, *i.e.*, adaptive feature block (AFeB), adaptive multi-scale block (AMB), and adaptive fusion block (AFuB). In brief, AFeB is designed to adaptively preserve image details and filter noises, which is highly expected for the features with mixed details and noises. AMB could enlarge the receptive field and aggregate the multi-scale information, which meets the need of contextually informative features. AFuB devotes to adaptively sampling and transferring the features from one scale to another scale, which fuses the multi-scale features with varying characteristics from coarse to fine. Extensive experiments on both three real and six synthetic noisy image datasets show the superiority of MSANet compared with 12 methods. The code could be accessed from https://github.com/XLearning-SCU/2022-NeurIPS-MSANet.

1 Introduction

In the real world, images are often contaminated by various signal-dependent or -independent noises during the image acquisition process. As a result, the imaging quality will deteriorate, thus hindering people and computers from receiving image information. To solve this problem, image denoising, as an essential step for image perception, has been extensively studied in the past decades [10, 19, 27, 50].

In the early, filtering-based methods remove the image noise by manually designing low-pass filters, *e.g.*, median filtering [8], bilateral filtering [36], and wiener filtering [7]. Afterward, model-based methods remove the image noise by optimizing a problem of maximum a posteriori [13, 40, 43]. For instance, ITS [40] proposed an intrinsic tensor sparsity regularization on the non-local similar image patches by assuming they could be sparsely represented. Looking from the other side, both the filtering- and model-based methods are based on image priors from the statistics of natural images, and thus could be referred to as prior-based methods. Although remarkable performance has been achieved, an unpleasant denoising result will be obtained once the priors are inconsistent with the real data distribution. To avoid prior engineering, learning-based methods adopt a data-driven fashion to remove noise by learning the mapping from the noisy image to the corresponding clean image.

*Corresponding author

36th Conference on Neural Information Processing Systems (NeurIPS 2022).

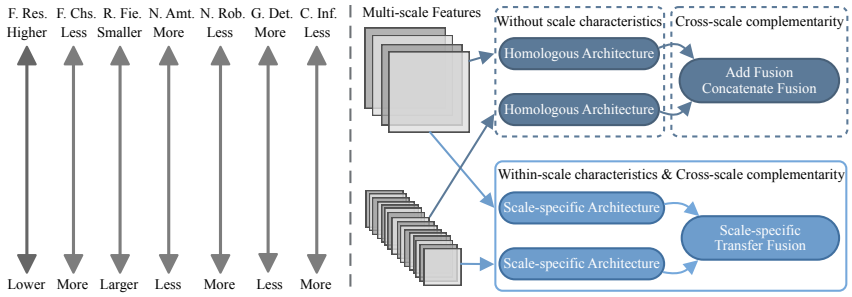

Figure 1: The motivations of MSANet. Left: the features at different resolutions show varying characteristics. In the figure, "F. Res." and "F. Chs." denote feature resolutions and channels, respectively; "R. Fie." denotes receptive field; "N. Amt." and "N. Rob." denote noise amount and robustness, respectively; "G. Det." and "C. Inf." denote geometric details and contextual information, respectively. Right: the major difference of MSANet with existing multi-scale architectures, *i.e.*, different scale features show varying characteristics and should be processed by scale-specific structures rather than homologous architectures.

With the popularity of deep neural networks, various network architectures have been designed and achieved state-of-the-art performance [6, 26, 32, 51]. For example, DnCNN [50] introduced residual learning and batch normalization to implement a denoising convolution network. SwinIR [19] introduced the shifted windowing scheme to implement a restoration Transformer network.

Among the network design paradigms, multi-scale architectures play a significant role in performance improvement thanks to multi-scale features. However, existing studies design their network architectures by only considering the cross-scale complementarity while ignoring the within-scale characteristics (see Fig. 1). To be exact, the shallow and high-resolution features, which lack awareness of contextual information, are sensitive to inputs and contain a lot of noises. Nevertheless, they contain abundant image geometric information, such as edges and textures. In consequence, they are critical for the recovery of fine-grained image details, and their network structures should take the advantages and make up for the disadvantages. The deep and low-resolution features are competitive in noise-robustness and contextual information, which are critical for the recovery of coarse-grained image context, but the too-low resolution destroys the image structure. Hence, their network structures should also make full consideration of their characteristics during the architecture design. To summarize, as different scale features show varying characteristics, it is deserved to deal with them via scale-specific structures to fully adapt to their characteristics.

Based on the motivation, we propose a novel Multi-Scale Adaptive Network (MSANet) for single image denoising, which simultaneously incorporates the within-scale characteristics and the cross-scale complementarity into architecture design by overcoming the following three difficulties, *i.e.*, i) how to adaptively sample image details and filter noises; ii) how to adaptively extract contextually informative features without changing feature resolutions; iii) how to adaptively fuse the multi-scale features with varying characteristics. Accordingly, three neural blocks, *i.e.*, adaptive feature block (AFeB), adaptive multi-scale block (AMB) and adaptive fusion block (AFuB) are proposed. In brief, AFeB handles the features with mixed details and noises through adaptively sampling and weighting, and thus the image details are preserved while filtering noises. AMB extracts the contextual information through dilated convolutions and adaptive aggregation, and thus contextually informative features are obtained while keeping the resolution. AFuB adaptively samples and transfers the features from one scale to another scale, and the multi-scale features with varying characteristics are fused from coarse to fine.

To summarize, the contributions are as follows:

- We propose a novel neural network for single image denoising, termed as MSANet. The major difference with existing methods is that MSANet simultaneously considers and incorporates the within-scale characteristics and the cross-scale complementarity into multi-scale architecture design, which is a missing piece before and the first revelation so far.
- To exploit the within-scale characteristics and achieve the cross-scale complementarity, we design three neural blocks, *i.e.*, AFeB, AMB, and AFuB, which are used to implement our

idea, *i.e.*, building scale-specific subnetworks corresponding to different scale features by considering their characteristics.

- Extensive experiments are conducted on three real and six synthetic noisy image datasets to show the effectiveness of MSANet, and the significance of the within-scale characteristics.

2 Related Work

In this section, we briefly introduce existing single image denoising methods and multi-scale architectures, and discuss the major differences between MSANet and them.

2.1 Single Image Denoising

In general, most existing single image denoising approaches could be categorized as prior- and learning-based methods. Prior-based methods are based on some priors from natural images, such as local smoothing [41], self-similarity [36, 10, 13], and sparsity [43, 40]. For instance, BM3D [10] eliminates noisy pixels by transforming the 3D stack of non-local similar patches and employing a shrinkage function to obtain sparse coefficients. WNNM [13] introduced a low-rank weight coefficient based on the nuclear norm minimization and exploited the non-local similar image patches to remove noise. Different from prior-based methods that heavily rely on handcrafted priors, learning-based methods learn the mapping from the noisy image to the clean image in an end-to-end manner. In recent, a large number of methods have been proposed and achieved state-of-the-art performance [6, 14, 32, 38, 47]. For example, MemNet [35] proposed a persistent memory network to fuse both short- and long-term memories for capturing different levels of information. FFDNet [51] enhanced the denoising network for non-uniform noise by using the noise level map. Non-local attention [37] was designed to exploit the image self-similarity, and NLRN [20] incorporated it into a recurrent neural network. SADNet [6] proposed residual spatial-adaptive block and multi-scale context block to constitute a denoising network. DeamNet [32] introduced an adaptive consistency prior and designed an interpretable deep denoising network. With the rise of vision Transformers, Uformer [38] proposed a U-shape Transformer based on the locally-enhanced window Transformer block and multi-scale restoration modulator. Restormer [47] introduced the channel-based self-attention and gating mechanism to implement an efficient Transformer.

Different from the aforementioned methods, MSANet proposed three neural blocks, *i.e.*, AFeB, AMB, and AFuB, by simultaneously considering the within-scale characteristics and the cross-scale complementarity, to constitute the scale-specific subnetworks corresponding to different scale features for adapting their varying characteristics.

2.2 Multi-Scale Architecture

Multi-scale architectures have played a significant role in many fields of computer vision [5, 17, 21, 48], thanks to multi-scale features and their cross-scale complementarity. The straightforward way for multi-scale architecture is to separately feed multi-/single-resolution images/features into single/multiple subnetworks, and then fuse the outputs as a result [18, 25, 39, 44, 45]. For example, HRNet [34] proposed a multi-scale network by gradually adding high-to-low resolution subnetworks and repeating multi-scale fusions for human pose estimation. CLEARER [12] proposed a multi-scale neural architecture search to automatically determine where to fuse multi-scale features for image restoration. GDN [22] exploited the multi-scale information using a grid-like network and employed an attention mechanism to improve the performance. DID-MDN [49] proposed a multi-stream densely connected network to efficiently leverage features of different scales for image deraining. MSCNN [33] consists of a coarse-scale network and a fine-scale network to learn a transmission map for image dehazing. PANet [25] proposed a pyramid attention network for image restoration by capturing long-range feature correspondences from a multi-scale feature pyramid. In addition, [6, 11, 38, 47] employed encoder-decoder architecture to combine the high-to-low with low-to-high resolution features through skip-connections.

Although the aforementioned studies and our work share similarities in multi-scale architecture, they are remarkably different. The existing methods only consider the cross-scale complementarity and use homologous architectures for different scale features. In contrast, our work additionally considers

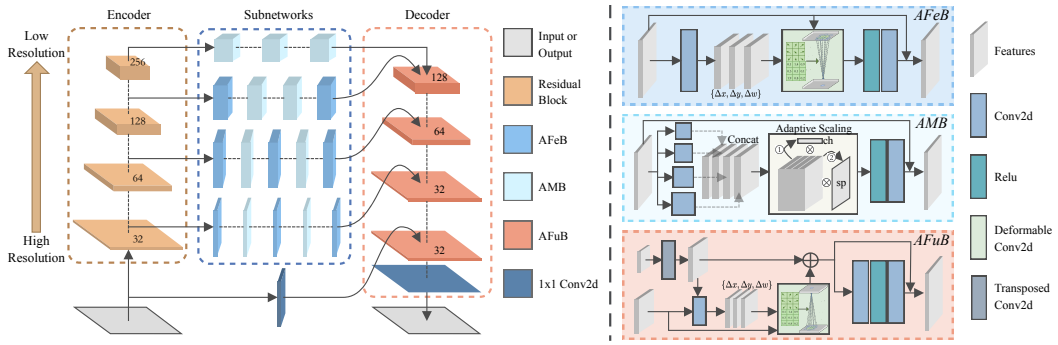

Figure 2: The framework of MSANet. It employs an asymmetric encoder-decoder architecture with multiple subnetworks to capture and fuse the scale-specific features. In addition, three neural blocks are designed to exploit the within-scale characteristics and achieve the cross-scale complementarity of multi-scale features. Note that we take four scales of features as a showcase and for experimental evaluations, more scales are allowed in practice.

the within-scale characteristics and designs scale-specific structures to embrace both, which is the missing piece and the first revelation for multi-scale architecture design.

3 Proposed Method

In this section, we propose a novel single image denoising network, *i.e.*, MSANet, which simultaneously embraces the within-scale characteristics and the cross-scale complementarity of multi-scale features through the three neural blocks. In the following, we will first introduce the architecture principles of MSANet and then elaborate on the three neural blocks.

3.1 Architecture Principles

As illustrated in Fig. 2, MSANet employs an asymmetric encoder-subnetworks-decoder architecture. Specifically, the encoder adopts four residual blocks [15] to extract features of four scales. The first residual block aims to extract the initial features without changing the resolution. The other residual blocks respectively decrease the resolutions to half while increasing the channels to double. With the multi-scale features extracted by the encoder, the subnetworks aim to exploit their within-scale characteristics via AFeB and AMB blocks. As the characteristics of multi-scale features gradually change from high- to low-resolution, we take the two bottom and two top subnetworks in Fig. 2 as the high- and low-resolution branches, respectively.

The two bottom subnetworks need to handle the high-resolution features which usually are characterized by a mixture of details and noises. It is highly expected to remove the noises without losing the fine-grained image details, and thus AFeB is designed for adaptively preserving the indispensable details and filtering unpleasant noises. Meanwhile, another characteristic of high-resolution features is the limited contextual information. The corresponding subnetworks should also enrich the contextual information while keeping the feature resolution unchanged in order not to lose details. As a result, AMB is designed for adaptively extracting contextually informative features. As AFeB and AMB could mutually boost each other, *i.e.*, low noise features from AFeB allow AMB to better capture the image contexts, while contextually informative features from AMB help AFeB to better distinguish the noises and details, we alternately stack AFeB and AMB to build the subnetworks. In addition, as the higher-resolution features usually have fewer channels (*i.e.*, fewer parameters), a deeper subnetwork is allowed to further alleviate their disadvantages, such as massive noises and limited contexts.

Different from the bottom subnetworks, the two top subnetworks aim to exploit the within-scale characteristics of the low-resolution features, which are characterized by less noise and more contextual information. As the too-low resolution will destroy the image structure, the structure consistency cannot be guaranteed during the image recovery. Hence, we employ AMB to capture more image contexts for enriching the contextual information without reducing the feature resolution. In addition,

as the low-resolution features are more robust to noise and have more channels, the top subnetworks mainly consist of AMB and are with shallower depth for efficiency. Meanwhile, except for the lowest resolution, the first and the last blocks in the top subnetworks are AFeB for adaptively controlling the input and output features.

To achieve the cross-scale complementarity, the decoder consists of four AFuB blocks followed by a convolution layer to output the recovered image. More specifically, the first three AFuB blocks increase the resolutions to double and decrease the channels to half, while adaptively sampling and transferring the fine-grained detail features to the coarse-grained contextual features. The last AFuB block keeps the resolution and channel unchanged, and directly samples and transfers the image details from the noisy input, which is an effective alternative to the global skip-connection, for which could avoid introducing noises from the noisy input.

For a given noisy input x, MSANet employs the encoder to extract the features of different scales and then feeds the features into different subnetworks to learn the scale-specific features. After that, the decoder fuses the multi-scale features with varying characteristics from coarse to fine to obtain the recovered image $\hat{y} = f(x)$, where $f(\cdot)$ denotes MSANet. To optimize MSANet, we employ the following objective function,

$$\mathcal{L} = \|y - \hat{y}\|_p^p \tag{1}$$

where y is the ground truth of x, and $p = \{1, 2\}$.

3.2 Adaptive Neural Blocks

In this section, we elaborate on the proposed three neural blocks which are designed to learn better multi-scale features for single image denoising.

Adaptive Feature Block (AFeB). To preserve the indispensable details and filter unpleasant noises, the block is expected to adaptively sample and weight the input features f_i based on themselves, *i.e.*,

$$\{\Delta x, \Delta y, \Delta w\}_{(x,y)} = F(f_i), \tag{2}$$

where $F(\cdot)$ is used to compute the offset $(\Delta x, \Delta y)$ w.r.t. the positions (x, y), as well as the corresponding weight Δw. Then, the output features f_{i+1} could be aggregated by

$$f_{i+1}(x, y) = \sum_{j=1}^{k} w_j * f_i(x + \Delta x_j, y + \Delta y_j) * \Delta w_j, \tag{3}$$

where k is the number of samples, and w denotes the learnable weights. In this way, AFeB could learn the sampling locations to indicate where are important for restoration, while assigning different weights to show how important the locations are. As a result, AFeB preserves the indispensable details and filters unpleasant noises for better restoration. However, it is prohibitive to traverse all positions for sampling and weighting w.r.t. each position in the input features. Hence, for the convenience of implementation, AFeB employs the modulated deformable convolution [55] to implement the aggregation operation in Eq.(3). In detail, AFeB sets the sample number to the kernel size and the learnable weights as the convolutional weights. Although this setting would decrease the number of samples and the flexibility of weights, it is efficient in the calculation of high-resolution features, and the limitations could be alleviated by stacking AFeB blocks. In summary, AFeB consists of a convolutional layer $F(\cdot)$, a modulated deformable convolution, a LeakyReLU layer, a convolutional layer and a skip-connection, *i.e.*,

$$f_{out} = f_i + F_{conv}(F_{relu}(f_{i+1})). \tag{4}$$

Adaptive Multi-scale Block (AMB). Contextually informative features are highly expected for both the high- and low-resolution branches. For the high-resolution features, reducing the resolution leads to the loss of image details. For low-resolution features, a too-low resolution destroys the structure consistency of recovered images. Therefore, to capture more contextual information without changing the resolution, we propose AMB by using several convolutions with different dilation rates. Convolution with a large dilation rate could provide a large receptive field, and multiple convolutions with different dilation rates could smoothly capture multi-scale information. To reduce the cost caused by the multiple convolutions, AMB compresses the channels of each convolution so that the concatenated channels of all convolutions are equal to the output channels, *i.e.*,

$$f_{i+1} = Concat(\{F_k^d(f_i) | d, k \in \mathbb{N}^+\}), \tag{5}$$

where f_i and f_{i+1} are input and output features, and F_k^d is the k-th convolution with the dilation rate d. As the concatenation assigns different scale features into different channels, the distinctive importance of multi-scale features is not considered. To address this issue, AMB adaptively scales different channels and features, *i.e.*,

$$\begin{aligned} ch &= 2 * F_{sig}(F_{fc}(avg_pool(f_{i+1}))), \\ f_{i+2} &= ch * f_{i+1}, \\ sp &= 2 * F_{sig}(F_{conv}(mean(f_{i+2}))), \\ f_{i+3} &= sp * f_{i+2}, \end{aligned} \tag{6}$$

where avg_pool is an adaptive average pooling on space domain, $mean$ denotes a mean operation along the channels, F_{fc} is a linear layer, F_{conv} is a convolutional layer, F_{sig} is a sigmoid layer, and $2*$ is used to control the amplification (> 1) or suppression (< 1). With the f_{i+3}, AMB passes it through a LeakyReLU layer, a convolutional layer and a skip-connection, *i.e.*,

$$f_{out} = f_i + F_{conv}(F_{relu}(f_{i+3})). \tag{7}$$

Adaptive Fusion Block (AFuB). As the high-resolution features contain a lot of disordered fine-grained image details, and the low-resolution features contain abundant coarse-grained image contextual information, it is desirable to transfer the fine-grained image details into the coarse-grained image context. To this end, AFuB first upsamples the coarse-grained features to the resolution of the fine-grained features via

$$f_{coarse} = F_{TConv}(f_{coarse}^{low}), \tag{8}$$

where F_{TConv} is a transpose convolution. Then, to address the issue of the disordered details, AFuB adaptively samples and weights the fine-grained features by using coarse-grained features to provide contextual information and fine-grained features to provide details information, *i.e.*,

$$\{\Delta x, \Delta y, \Delta w\}_{(x,y)} = F(f_{coarse}, f_{fine}), \tag{9}$$

where $F(\cdot,\cdot)$ is used to compute the offset $(\Delta x, \Delta y)$ w.r.t. the positions (x, y), as well as the corresponding weight Δw. After that, AFuB transfers the fine-grained details to the coarse-grained context via

$$f_{coarse}^{fine} = f_{coarse} + \sum_{j=1}^{k} w_j * f_{fine}(x + \Delta x_j, y + \Delta y_j) * \Delta w_j, \tag{10}$$

where k is the number of fine-grained detail features, w is the learnable weights. Similar to AFeB, AFuB employs a convolutional layer as the function F and a modulated deformable convolution to achieve the aggregation in Eq.(10). Finally, AFuB uses a convolutional layer, a LeakyReLU layer, a convolutional layer, and a skip-connection for further refining features, *i.e.*,

$$f_{out} = f_{coarse}^{fine} + F_{conv}(F_{relu}(F_{conv}(f_{coarse}^{fine}))). \tag{11}$$

4 Experiments

In this section, we first introduce the experimental settings, and then show the quantitative and qualitative results on nine datasets. Finally, we perform analysis experiments including ablation study and feature-based visualization. Due to space limitations, we present more experimental details and results in the supplementary material.

4.1 Experimental settings

We evaluate the MSANet on both real and synthetic noisy datasets. For the evaluations on real noise, we employ the SIDD [1], RENOIR [3], Poly [42] datasets for training, and use SIDD Validation, Nam [28] and DnD [30] datasets for testing. For synthetic noise, we train MSANet on DIV2K [2] dataset, which contains 800 images of 2K resolution, by adding Additive White Gaussian Noise (AWGN) with the noise levels of 30, 50, and 70. We use color McMaster [52] (CMcMaster), color Kodak24 (CKodak24), color BSD68 [24] (CBSD68) for testing color image denoising, and grayscale McMaster (GMcMaster), grayscale Kodak24 (GKodak24), grayscale BSD68 (GBSD68) for testing grayscale image denoising.

We implement MSANet in Pytorch [29] and carry out all experiments on Ubuntu 20.04 with GeForce RTX 3090 GPUs. In our implementations, we use four scales of features with channels of 32, 64, 128 and 256. Moreover, we train MSANet 100 epochs via L_1 loss for real noise and 300 epochs via L_2 loss for synthetic noise. Both real and synthetic noise training are with the batch size of 16 and the patch size of 128. To optimize MSANet, the Adam [16] optimizer is used, and the learning rate is initially set to 1e-4 and decays to zero via the cosine annealing strategy [23]. During the training, we randomly crop, flip and rotate the patches for data augmentation. In the testing, we employ PSNR and SSIM to evaluate the performance.

4.2 Comparisons on Real Noise Images

Table 1: Quantitative results on SIDD sRGB validation dataset.

Method	CDnCNN-B	CBM3D	CBDNet	PD	RIDNet	SADNet	DeamNet	MSANet
PSNR	26.21	30.88	33.07	33.96	38.71	39.46	39.47	**39.56**
SSIM	-	-	0.8324	0.8195	0.9052	0.9103	0.9105	**0.9118**

Table 2: Quantitative results on Nam dataset with JPEG compression.

Method	CDnCNN-B	CBM3D	CBDNet	PD	RIDNet	SADNet	DeamNet	MSANet
PSNR	37.49	39.84	41.31	41.09	41.04	42.92	42.03	**43.52**
SSIM	0.9272	0.9657	0.9784	0.9780	0.9814	0.9839	0.9790	**0.9863**

Table 3: Quantitative results on DnD sRGB dataset.

Method	CDnCNN-B	CBM3D	FFDNet+	CBDNet	N3Net	PR	RIDNet	SADNet	DeamNet	MSANet
PSNR	32.43	34.51	37.61	38.06	38.32	39.00	39.26	39.59	39.63	**39.65**
SSIM	0.7900	0.8507	0.9415	0.9421	0.9384	0.9542	0.9528	0.9523	0.9531	**0.9553**

Real noise image denoising is challenging due to the real noise being usually signal-dependent and spatial-variant hinges on the in-camera pipeline. Therefore, we carry out denoising experiments on three real noise image datasets, *i.e.*, SIDD Validation, Nam, and DnD. In brief, the validation dataset of SIDD contains 1,280 256×256 noisy-clean image pairs captured by the smartphone. Nam includes 15 large image pairs with JPEG compression, and we evaluate MSANet on the selected 25 512×512 patches by following CBDNet [14]. DnD contains 50 pairs of real noisy-clean images captured by cameras, and 1,000 512×512 patches are extracted for testing. Due to the ground truths of the patches are not publicly available, we obtain the PSNR and SSIM results via the online submission system [30]. Besides, since JPEG compression makes the noise more stubborn on the Nam, we first train our model on the combination of SIDD and RENOIR for the evaluations on SIDD Validation and DND, and then fine-tune the trained model on the Poly for the evaluations on Nam.

We compare MSANet with 10 denoising methods that are comparable in model complexity, *i.e.*, CDnCNN-B, CBM3D [9], FFDNet+, CBDNet, N3Net [31], PD [54], PR [46], RIDNet [4], SADNet and DeamNet. In experiments, we use the corresponding pretrained models provided by their authors, and refer to their results reported in the online submission system and papers.

Table 1 shows the quantitative results on SIDD validation dataset. In brief, MSANet achieves the highest PSNR and SSIM values compared to other methods, *e.g.*, 0.85dB, 0.1dB, 0.09dB gains in PSNR, and 0.0066, 0.0015, 0.0013 gains in SSIM over the RIDNet, SADNet, and DeamNet, respectively. For visual comparisons in Fig. 3, CBDNet and PD result in residual noises and pseudo artifacts, RIDNet, SADNet and DeamNet severely destroy the textures and obtain over-smoothed results. In contrast, our method MSANet recovers textures and structures more subtly and obtains clearer restoration. Some areas are highlighted by color rectangles and zooming-in is recommended for better visualization.

The quantitative results on Nam dataset are shown in Table 2, which demonstrates that our method achieves significant improvements over the other methods. Specifically, MSANet outperforms RIDNet with 2.48dB (0.0049), SADNet with 0.6dB (0.0024), DeamNet with 1.49dB (0.0073) in PSNR (SSIM) values. For the visual comparisons shown in Fig. 4, our method obtains the best result for details recovery and noises removal, which is closer to the ground truth than other results.

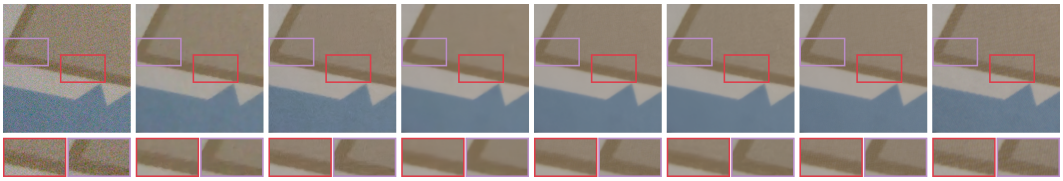

Figure 3: Qualitative results on real noise image from SIDD validation dataset. From left to right, we show the real noise image, the results of CBDNet, PD, RIDNet, SADNet, DeamNet, MSANet, and the ground truth.

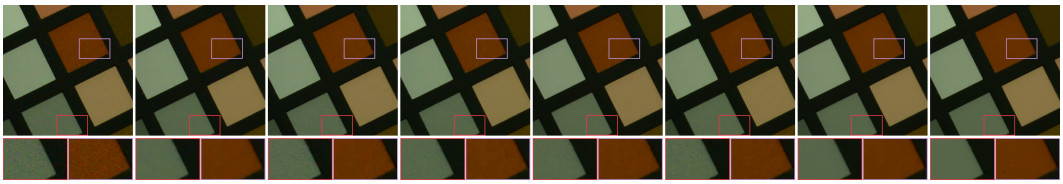

Figure 4: Qualitative results on real noise image from Nam dataset. From left to right, we show the real noise image, the results of CBDNet, PD, RIDNet, SADNet, DeamNet, MSANet, and the ground truth.

Figure 5: Qualitative results on real noise image from DnD dataset. From left to right, we show the real noise image, the results of CBDNet, RIDNet, PD, SADNet, DeamNet, and MSANet.

Table 3 reports the quantitative results on DnD dataset, which are obtained from the DnD benchmark website. From the table, one could observe that MSANet outperforms all methods both in PSNR and SSIM values. Moreover, we further perform a qualitative comparison on the DnD dataset. As shown in Fig. 5, the other methods achieve blurred results wherein many image details are corroded by noises, while our method can effectively remove the noises and obtain clearer details.

4.3 Comparisons on Synthetic Noise Images

Table 4: Quantitative results on synthetic color noise image datasets.

Dataset	σ	CBM3D	DnCNN	FFDNet	CLEARER	SADNet	RNAN	DeamNet	MSANet (Ours)
CMcMaster	30	29.58/0.8107	29.64/0.8098	30.05/0.8221	30.83/0.8522	31.96/0.8857	32.01/0.8848	32.00/0.8862	**32.07/0.8876**
	50	25.92/0.7153	25.99/0.7147	26.23/0.7244	28.92/0.8143	29.72/0.8374	29.69/0.8333	29.78/0.8393	**29.82/0.8403**
	70	23.12/0.6398	23.03/0.6297	23.19/0.6406	26.96/0.7504	28.25/0.7988	28.14/0.7918	28.27/0.8000	**28.35/0.8028**
CKodak24	30	30.33/0.8417	30.77/0.8548	30.62/0.8542	31.17/0.8590	31.72/0.8730	31.72/0.8716	31.76/0.8736	**31.78/0.8744**
	50	27.28/0.7572	27.63/0.7718	27.54/0.7687	28.94/0.7977	29.49/0.8149	29.43/0.8102	29.53/0.8155	**29.57/0.8169**
	70	24.84/0.6890	24.90/0.6912	24.88/0.6890	27.59/0.7503	28.10/0.7715	27.99/0.7635	28.14/0.7721	**28.17/0.7731**
CBSD68	30	29.22/0.8378	29.72/0.8556	29.51/0.8526	30.35/0.8665	30.63/0.8749	30.61/0.8733	30.65/0.8749	**30.67/0.8758**
	50	26.06/0.7378	26.48/0.7600	26.38/0.7550	28.01/0.7996	28.31/0.8089	28.25/0.8050	28.34/0.8093	**28.36/0.8107**
	70	23.70/0.6548	23.86/0.6626	23.80/0.6584	26.58/0.7433	26.91/0.7577	26.81/0.7511	26.92/0.7574	**26.96/0.7591**

We carry out experiments on three color and three grayscale noisy image datasets. Specifically, the datasets are obtained by adding AWGN with the levels of 30, 50, and 70 to the color and grayscale version of BSD68, Kodak24 and McMaster, respectively. In brief, BSD68 contains 68 images which are frequently used for measuring image denoising performance, Kodak24 contains 24 images captured by film cameras, and McMaster contains 18 images with statistics closer to natural images.

For comparisons, we choose seven representative denoising methods, *i.e.*, BM3D [10], DnCNN [50], FFDNet [51], CLEARER [12], RNAN [53], SADNet [6] and DeamNet [32]. We call the python

Table 5: Quantitative results on synthetic grayscale noise image datasets.

Dataset	σ	BM3D	DnCNN	FFDNet	CLEARER	SADNet	RNAN	DeamNet	MSANet (Ours)
GMcMaster	30	29.45/0.8151	29.80/0.8119	29.89/0.8292	30.29/0.8491	30.92/0.8649	30.92/0.8629	30.94/0.8656	**30.96/0.8661**
	50	26.23/0.7218	26.24/0.7281	26.46/0.7319	28.31/0.7945	28.61/0.8052	28.57/0.8014	28.65/0.8070	**28.68/0.8072**
	70	23.78/0.6517	23.63/0.6682	23.64/0.6466	26.83/0.7427	27.18/0.7606	27.06/0.7526	27.20/0.7616	**27.22/0.7620**
GKodak24	30	28.71/0.7854	29.21/0.7946	29.15/0.8077	29.49/0.8132	29.87/0.8238	29.89/0.8208	29.90/0.8241	**29.91/0.8248**
	50	26.22/0.6996	26.52/0.7190	26.52/0.7177	27.27/0.7412	27.77/0.7559	27.73/0.7494	27.79/**0.7567**	**27.81**/0.7564
	70	24.37/0.6393	24.31/0.6647	24.28/0.6419	26.12/0.6931	26.51/0.7090	26.42/0.6989	26.53/**0.7107**	**26.54**/0.7091
GBSD68	30	27.43/0.7721	27.96/0.7762	27.89/0.7982	28.27/0.8112	28.58/0.8165	28.59/0.8140	28.59/0.8165	**28.61/0.8174**
	50	24.90/0.6715	25.19/0.6826	25.19/0.6909	26.09/0.7295	26.50/0.7382	26.46/0.7333	26.50/0.7392	**26.51/0.7393**
	70	23.07/0.5985	23.04/0.6107	22.98/0.5942	25.03/0.6734	25.23/0.6828	25.15/0.6736	25.23/**0.6831**	**25.25**/0.6826

library for the evaluation of BM3D, and the pretrained models, provided by authors or retrained by us, for the evaluations of the other methods.

Table 4 reports the quantitative results on color image denoising, which shows that MSANet achieves the highest PSNR and SSIM values. Taking the noise level of 70 as an example, our method can achieve PSNR gains about $0.03 \sim 0.27$dB, and SSIM gains about $0.0010 \sim 0.0111$ over the state-of-the-art methods, *i.e.*, SADNet, RNAN, and DeamNet. Table 5 shows the quantitative results on grayscale image denoising. From the table, one could observe that MSANet achieves the highest PSNR values, and outperforms the other methods about $0.01 \sim 3.59$dB w.r.t. PSNR.

4.4 Analysis Experiments

The ablation study is conducted to demonstrate the significance of utilizing the within-scale characteristics (WSC) and the cross-scale complementarity (CSC). As shown in Table 6, "ED" and "ResB" are with homologous architectures, which use uniform Identity Mapping and Residual Block to process different scale features, respectively. As using AFeB and AMB alone cannot exploit WSC well, "AFeB"/"AMB" and "AFeB+AFuB"/"AMB+AFuB" only slightly improve the performance over "ResB" and "AFuB", respectively. When using AFeB and AMB together, "AFeB+AMB" and MSANet (*i.e.*, "AFeB+AMB+AFuB") significantly improve the performance over "ResB" and "AFuB", verifying our claim on the role of AFeB+AMB w.r.t. WSC. Furthermore, thanks to CSC through AFuB, "AFuB" and MSANet ("AFeB+AMB+AFuB") are significantly better than "ResB" and "AFeB+AMB", respectively. In summary, the ablation study not only demonstrates the significance of well utilizing WSC and CSC, but also shows the effectiveness of our proposed solution.

Table 6: Ablation study on CMcMaster with the noise level of 30. "ED" denotes the encoder-decoder architecture with skip connections. "ResB" denotes to substitute the blocks in MSANet with the residual blocks. "AFeB", "AMB", "AFuB", "AFeB+AMB", "AFeB+AFuB" and "AMB+AFuB" denote to use the corresponding blocks on the basis of "ResB".

Ablations	ED	ResB	AFeB	AMB	AFuB	AFeB+AMB	AFeB+AFuB	AMB+AFuB	MSANet
PSNR	31.70	31.93	31.94	31.94	32.01	31.98	32.04	32.03	32.07
SSIM	0.8801	0.8851	0.8854	0.8851	0.8864	0.8860	0.8869	0.8866	0.8876

To further demonstrate the significance of the within-scale characteristics, and the effectiveness of our solution in exploiting it, we show the qualitative comparisons on the intermediate multi-scale features before (*i.e.*, without) and after (*i.e.*, with) our subnetworks in MSANet. From the Fig. 6, one could observe that our subnetworks could well exploit the within-scale characteristics, *i.e.*, preserving the indispensable details while filtering the unpleasant noises for high-resolution features (*i.e.*, 2nd and 3rd columns), and capturing rich contextual information for low-resolution features (*i.e.*, 4th and 5th columns). Besides, the different scale features show varying characteristics and significant cross-scale complementarity, which would be further exploited by our AFuB.

5 Conclusions

In this paper, we proposed MSANet with three neural blocks, *i.e.*, AFeB, AMB, and AFuB, for single image denoising. Different from existing multi-scale architectures, MSANet considers not only the cross-scale complementarity but also the within-scale characteristics, thus boosting the recovery performance as verified in experiments. As this work could be regarded as finding the missing piece

Figure 6: Qualitative comparisons on the intermediate multi-scale features in MSANet. The top left is the noise image, and the bottom left is the corresponding clean image. From left to right, the feature resolution varies from high to low. The top row is the features before (*i.e.*, without) subnetworks, and the bottom row is the features after (*i.e.*, with) subnetworks.

of multi-scale architecture design, we will explore other solutions to simultaneously exploit the within-scale characteristics and the cross-scale complementarity, and investigate their effectiveness in broader tasks such as deblur, segmentation.

Broader Impact Statement. MSANet is a specifically designed architecture for supervised single image denoising, which requires intensive labor to collect a lot of noisy-clean image pairs, and thus has the potential to make more opportunities for employment. However, MSANet is a general neural network and might be trained with uncertain data and used for uncertain purposes, such as watermark removal, which might prejudice the rights of others. Besides, MSANet involves a novel idea of multi-scale architecture design and might be used to design new networks for uncertain purposes. Moreover, the training and running of the model consume a lot of electricity causing carbon emission.

Acknowledgements

This work was supported in part by NSFC under Grant U21B2040, U19A2078, and 61836006; and in part by Sichuan Science and Technology Planning Project under Grant 2022YFQ0014.

References

[1] Abdelrahman Abdelhamed, Stephen Lin, and Michael S Brown. A high-quality denoising dataset for smartphone cameras. In *IEEE Conf. Comput. Vis. Pattern Recog.*, pages 1692–1700, 2018.

[2] Eirikur Agustsson and Radu Timofte. Ntire 2017 challenge on single image super-resolution: dataset and study. In *IEEE Conf. Comput. Vis. Pattern Recog. Worksh.*, July 2017.

[3] Josue Anaya and Adrian Barbu. Renoir–a dataset for real low-light image noise reduction. *Journal of Visual Communication and Image Representation*, 51:144–154, 2018.

[4] Saeed Anwar and Nick Barnes. Real image denoising with feature attention. In *Int. Conf. Comput. Vis.*, pages 3155–3164, 2019.

[5] Xiaochun Cao, Wenqi Ren, Wangmeng Zuo, Xiaojie Guo, and Hassan Foroosh. Scene text deblurring using text-specific multiscale dictionaries. *IEEE Trans. Image Process.*, 24(4):1302–1314, 2015.

[6] Meng Chang, Qi Li, Huajun Feng, and Zhihai Xu. Spatial-adaptive network for single image denoising. In *Eur. Conf. Comput. Vis.*, pages 171–187. Springer, 2020.

[7] Jingdong Chen, Jacob Benesty, Yiteng Huang, and Simon Doclo. New insights into the noise reduction wiener filter. *IEEE Trans. on Audio, Speech, and Language Process.*, 14(4):1218–1234, 2006.

[8] Tao Chen, Kai-Kuang Ma, and Li-Hui Chen. Tri-state median filter for image denoising. *IEEE Trans. Image Process.*, 8(12):1834–1838, 1999.

[9] Kostadin Dabov, Alessandro Foi, Vladimir Katkovnik, and Karen Egiazarian. Color image denoising via sparse 3d collaborative filtering with grouping constraint in luminance-chrominance space. In *IEEE Int. Conf. Image Process.*, volume 1, pages I–313. IEEE, 2007.

[10] Kostadin Dabov, Alessandro Foi, Vladimir Katkovnik, and Karen Egiazarian. Image denoising by sparse 3-d transform-domain collaborative filtering. *IEEE Trans. Image Process.*, 16(8):2080–2095, 2007.

[11] Hang Dong, Jinshan Pan, Lei Xiang, Zhe Hu, Xinyi Zhang, Fei Wang, and Ming-Hsuan Yang. Multi-scale boosted dehazing network with dense feature fusion. In *IEEE Conf. Comput. Vis. Pattern Recog.*, June 2020.

[12] Yuanbiao Gou, Boyun Li, Zitao Liu, Songfan Yang, and Xi Peng. Clearer: Multi-scale neural architecture search for image restoration. *Adv. Neural Inform. Process. Syst.*, 33, 2020.

[13] Shuhang Gu, Lei Zhang, Wangmeng Zuo, and Xiangchu Feng. Weighted nuclear norm minimization with application to image denoising. In *IEEE Conf. Comput. Vis. Pattern Recog.*, pages 2862–2869, 2014.

[14] Shi Guo, Zifei Yan, Kai Zhang, Wangmeng Zuo, and Lei Zhang. Toward convolutional blind denoising of real photographs. In *IEEE Conf. Comput. Vis. Pattern Recog.*, June 2019.

[15] Kaiming He, Xiangyu Zhang, Shaoqing Ren, and Jian Sun. Deep residual learning for image recognition. In *IEEE Conf. Comput. Vis. Pattern Recog.*, pages 770–778, 2016.

[16] Diederik P Kingma and Jimmy Ba. Adam: A method for stochastic optimization. *arXiv preprint arXiv:1412.6980*, 2014.

[17] Boyun Li, Yuanbiao Gou, Shuhang Gu, Jerry Zitao Liu, Joey Tianyi Zhou, and Xi Peng. You only look yourself: Unsupervised and untrained single image dehazing neural network. *Int. J. Comput. Vis.*, 129(5):1754–1767, 2021.

[18] Boyun Li, Yuanbiao Gou, Jerry Zitao Liu, Hongyuan Zhu, Joey Tianyi Zhou, and Xi Peng. Zero-shot image dehazing. *IEEE Trans. Image Process.*, 29:8457–8466, 2020.

[19] Jingyun Liang, Jiezhang Cao, Guolei Sun, Kai Zhang, Luc Van Gool, and Radu Timofte. Swinir: Image restoration using swin transformer. In *Int. Conf. Comput. Vis. Worksh.*, October 2021.

[20] Ding Liu, Bihan Wen, Yuchen Fan, Chen Change Loy, and Thomas S Huang. Non-local recurrent network for image restoration. In *Adv. Neural Inform. Process. Syst.*, pages 1680–1689, 2018.

[21] Jinyuan Liu, Xin Fan, Ji Jiang, Risheng Liu, and Zhongxuan Luo. Learning a deep multi-scale feature ensemble and an edge-attention guidance for image fusion. *IEEE Trans. Circuit Syst. Video Technol.*, 2021.

[22] Xiaohong Liu, Yongrui Ma, Zhihao Shi, and Jun Chen. Griddehazenet: Attention-based multi-scale network for image dehazing. In *IEEE Conf. Comput. Vis. Pattern Recog.*, pages 7314–7323, 2019.

[23] Ilya Loshchilov and Frank Hutter. Sgdr: Stochastic gradient descent with warm restarts. *arXiv preprint arXiv:1608.03983*, 2016.

[24] David Martin, Charless Fowlkes, Doron Tal, and Jitendra Malik. A database of human segmented natural images and its application to evaluating segmentation algorithms and measuring ecological statistics. In *Int. Conf. Comput. Vis.*, volume 2, pages 416–423. IEEE, 2001.

[25] Yiqun Mei, Yuchen Fan, Yulun Zhang, Jiahui Yu, Yuqian Zhou, Ding Liu, Yun Fu, Thomas S Huang, and Humphrey Shi. Pyramid attention networks for image restoration. *arXiv preprint arXiv:2004.13824*, 2020.

[26] Chong Mou, Qian Wang, and Jian Zhang. Deep generalized unfolding networks for image restoration. In *IEEE Conf. Comput. Vis. Pattern Recog.*, 2022.

[27] Chong Mou and Jian Zhang. Graph attention neural network for image restoration. In *Int. Conf. Multimedia and Expo*, pages 1–6, 2021.

[28] Seonghyeon Nam, Youngbae Hwang, Yasuyuki Matsushita, and Seon Joo Kim. A holistic approach to cross-channel image noise modeling and its application to image denoising. In *IEEE Conf. Comput. Vis. Pattern Recog.*, pages 1683–1691, 2016.

[29] Adam Paszke, Sam Gross, Francisco Massa, Adam Lerer, James Bradbury, Gregory Chanan, Trevor Killeen, Zeming Lin, Natalia Gimelshein, Luca Antiga, et al. Pytorch: An imperative style, high-performance deep learning library. *Adv. Neural Inform. Process. Syst.*, 32:8026–8037, 2019.

[30] Tobias Plotz and Stefan Roth. Benchmarking denoising algorithms with real photographs. In *IEEE Conf. Comput. Vis. Pattern Recog.*, pages 1586–1595, 2017.

[31] Tobias Plötz and Stefan Roth. Neural nearest neighbors networks. *Adv. Neural Inform. Process. Syst.*, 31:1087–1098, 2018.

[32] Chao Ren, Xiaohai He, Chuncheng Wang, and Zhibo Zhao. Adaptive consistency prior based deep network for image denoising. In *IEEE Conf. Comput. Vis. Pattern Recog.*, pages 8596–8606, 2021.

[33] Wenqi Ren, Jinshan Pan, Hua Zhang, Xiaochun Cao, and Ming-Hsuan Yang. Single image dehazing via multi-scale convolutional neural networks with holistic edges. *Int. J. Comput. Vis.*, 128(1):240–259, 2020.

[34] Ke Sun, Bin Xiao, Dong Liu, and Jingdong Wang. Deep high-resolution representation learning for human pose estimation. In *IEEE Conf. Comput. Vis. Pattern Recog.*, June 2019.

[35] Ying Tai, Jian Yang, Xiaoming Liu, and Chunyan Xu. Memnet: A persistent memory network for image restoration. In *Int. Conf. Comput. Vis.*, pages 4539–4547, 2017.

[36] Carlo Tomasi and Roberto Manduchi. Bilateral filtering for gray and color images. In *Int. Conf. Comput. Vis.*, pages 839–846. IEEE, 1998.

[37] Xiaolong Wang, Ross Girshick, Abhinav Gupta, and Kaiming He. Non-local neural networks. In *IEEE Conf. Comput. Vis. Pattern Recog.*, pages 7794–7803, 2018.

[38] Zhendong Wang, Xiaodong Cun, Jianmin Bao, Wengang Zhou, Jianzhuang Liu, and Houqiang Li. Uformer: A general u-shaped transformer for image restoration. In *IEEE Conf. Comput. Vis. Pattern Recog.*, pages 17683–17693, June 2022.

[39] Wenhao Wu, Yuxiang Zhao, Yanwu Xu, Xiao Tan, Dongliang He, Zhikang Zou, Jin Ye, Yingying Li, Mingde Yao, Zichao Dong, et al. Dsanet: Dynamic segment aggregation network for video-level representation learning. In *ACM Int. Conf. Multimedia*, pages 1903–1911, 2021.

[40] Qi Xie, Qian Zhao, Deyu Meng, Zongben Xu, Shuhang Gu, Wangmeng Zuo, and Lei Zhang. Multispectral images denoising by intrinsic tensor sparsity regularization. In *IEEE Conf. Comput. Vis. Pattern Recog.*, pages 1692–1700, 2016.

[41] Jinjun Xu and Stanley Osher. Iterative regularization and nonlinear inverse scale space applied to wavelet-based denoising. *IEEE Trans. Image Process.*, 16(2):534–544, 2007.

[42] Jun Xu, Hui Li, Zhetong Liang, David Zhang, and Lei Zhang. Real-world noisy image denoising: A new benchmark. *arXiv preprint arXiv:1804.02603*, 2018.

[43] Jun Xu, Lei Zhang, and David Zhang. A trilateral weighted sparse coding scheme for real-world image denoising. In *Eur. Conf. Comput. Vis.*, pages 20–36, 2018.

[44] Ruikang Xu, Zeyu Xiao, Jie Huang, Yueyi Zhang, and Zhiwei Xiong. Edpn: Enhanced deep pyramid network for blurry image restoration. In *IEEE Conf. Comput. Vis. Pattern Recog.*, pages 414–423, 2021.

[45] Hongyu Yang, Di Huang, Yunhong Wang, and Anil K. Jain. Learning face age progression: A pyramid architecture of gans. In *IEEE Conf. Comput. Vis. Pattern Recog.*, June 2018.

[46] Ke Yu, Xintao Wang, Chao Dong, Xiaoou Tang, and Chen Change Loy. Path-restore: Learning network path selection for image restoration. *IEEE Trans. Pattern Anal. Mach. Intell.*, 2021.

[47] Syed Waqas Zamir, Aditya Arora, Salman Khan, Munawar Hayat, Fahad Shahbaz Khan, and Ming-Hsuan Yang. Restormer: Efficient transformer for high-resolution image restoration. In *IEEE Conf. Comput. Vis. Pattern Recog.*, pages 5728–5739, June 2022.

[48] Syed Waqas Zamir, Aditya Arora, Salman Khan, Munawar Hayat, Fahad Shahbaz Khan, Ming-Hsuan Yang, and Ling Shao. Multi-stage progressive image restoration. In *IEEE Conf. Comput. Vis. Pattern Recog.*, pages 14821–14831, 2021.

[49] He Zhang and Vishal M Patel. Density-aware single image de-raining using a multi-stream dense network. In *IEEE Conf. Comput. Vis. Pattern Recog.*, pages 695–704, 2018.

[50] Kai Zhang, Wangmeng Zuo, Yunjin Chen, Deyu Meng, and Lei Zhang. Beyond a gaussian denoiser: Residual learning of deep cnn for image denoising. *IEEE Trans. Image Process.*, 26(7):3142–3155, 2017.

[51] Kai Zhang, Wangmeng Zuo, and Lei Zhang. Ffdnet: Toward a fast and flexible solution for cnn-based image denoising. *IEEE Trans. Image Process.*, 27(9):4608–4622, 2018.

[52] Lei Zhang, Xiaolin Wu, Antoni Buades, and Xin Li. Color demosaicking by local directional interpolation and nonlocal adaptive thresholding. *Journal of Electronic Imaging*, 20(2):023016, 2011.

[53] Yulun Zhang, Kunpeng Li, Kai Li, Bineng Zhong, and Yun Fu. Residual non-local attention networks for image restoration. In *Int. Conf. Learn. Represent.*, 2019.

[54] Yuqian Zhou, Jianbo Jiao, Haibin Huang, Yang Wang, Jue Wang, Honghui Shi, and Thomas Huang. When awgn-based denoiser meets real noises. In *AAAI*, volume 34, pages 13074–13081, 2020.

[55] Xizhou Zhu, Han Hu, Stephen Lin, and Jifeng Dai. Deformable convnets v2: More deformable, better results. In *IEEE Conf. Comput. Vis. Pattern Recog.*, pages 9308–9316, 2019.

Checklist

1. For all authors...
   (a) Do the main claims made in the abstract and introduction accurately reflect the paper's contributions and scope? [Yes]
   (b) Did you describe the limitations of your work? [Yes]
   (c) Did you discuss any potential negative societal impacts of your work? [Yes] See Broader Impact Statement.
   (d) Have you read the ethics review guidelines and ensured that your paper conforms to them? [Yes]
2. If you are including theoretical results...
   (a) Did you state the full set of assumptions of all theoretical results? [N/A]
   (b) Did you include complete proofs of all theoretical results? [N/A]
3. If you ran experiments...
   (a) Did you include the code, data, and instructions needed to reproduce the main experimental results (either in the supplemental material or as a URL)? [Yes] See the URL of Github in Abstract.

(b) Did you specify all the training details (e.g., data splits, hyperparameters, how they were chosen)? [Yes]

(c) Did you report error bars (e.g., with respect to the random seed after running experiments multiple times)? [No]

(d) Did you include the total amount of compute and the type of resources used (e.g., type of GPUs, internal cluster, or cloud provider)? [Yes]

4. If you are using existing assets (e.g., code, data, models) or curating/releasing new assets...

   (a) If your work uses existing assets, did you cite the creators? [Yes]

   (b) Did you mention the license of the assets? [Yes] It is detailed in the source code.

   (c) Did you include any new assets either in the supplemental material or as a URL? [No]

   (d) Did you discuss whether and how consent was obtained from people whose data you're using/curating? [No] We use the public datasets in our experiments.

   (e) Did you discuss whether the data you are using/curating contains personally identifiable information or offensive content? [N/A] We conduct experiments on the public datasets, which are widely used for research. The discussion of personally identifiable information or offensive content could be referred to the data publisher.

5. If you used crowdsourcing or conducted research with human subjects...

   (a) Did you include the full text of instructions given to participants and screenshots, if applicable? [N/A]

   (b) Did you describe any potential participant risks, with links to Institutional Review Board (IRB) approvals, if applicable? [N/A]

   (c) Did you include the estimated hourly wage paid to participants and the total amount spent on participant compensation? [N/A]